

Stable Segment Anything Model

Qi Fan¹, Xin Tao², Lei Ke³, Mingqiao Ye³, Yuan Zhang², Pengfei Wan²,
Zhongyuan Wang², Yu-Wing Tai⁴, Chi-Keung Tang¹

¹ The Hong Kong University of Science and Technology,

² Kuaishou Technology, ³ ETH Zurich, ⁴ Dartmouth College

<https://github.com/fanq15/Stable-SAM>

Abstract

The Segment Anything Model (SAM) achieves remarkable promptable segmentation given high-quality prompts which, however, often require good skills to specify. To make SAM robust to casual prompts, this paper presents the first comprehensive analysis on SAM’s segmentation stability across a diverse spectrum of prompt qualities, notably imprecise bounding boxes and insufficient points. Our key finding reveals that given such low-quality prompts, SAM’s mask decoder tends to activate image features that are biased towards the background or confined to specific object parts. To mitigate this issue, our key idea consists of adjusting the sampling locations of image feature using learnable deformable offsets, while the original SAM model architecture and weights remain unchanged. Consequently, our deformable sampling plugin (DSP) enables SAM to adaptively shift attention to the prompted target regions in a data-driven manner. During inference, dynamic routing plugin (DRP) is proposed that toggles SAM between the deformable and regular grid sampling modes, conditioned on the input prompt quality. Thus, our solution, termed Stable-SAM, is one of its kind focusing on solely adjusting feature sampling locations, which offers several advantages: 1) improved SAM’s segmentation stability across a wide range of prompt qualities, while 2) retaining SAM’s powerful promptable segmentation efficiency and generality, with 3) minimal learnable parameters (0.08 M) and fast adaptation. Extensive experiments validate the effectiveness and advantages of our approach, underscoring Stable-SAM as a more robust solution for segmenting anything.

1. Introduction

The recent Segment Anything Model (SAM [35]) stands a significant milestone in image segmentation, attributed to

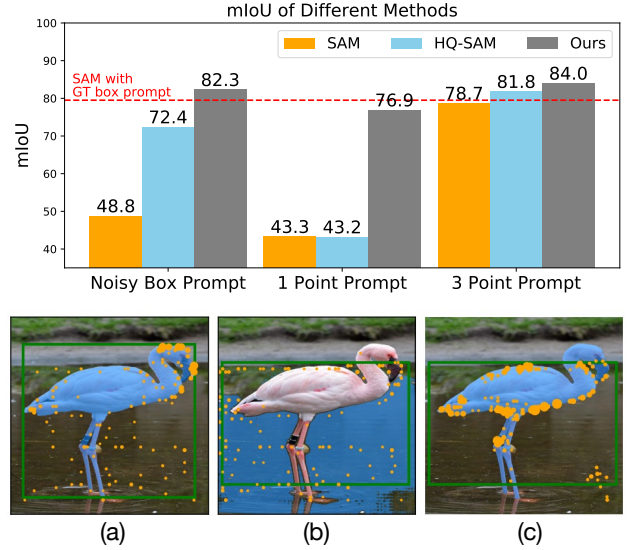


Figure 1. The top row shows a performance comparison among SAM, HQ-SAM and our Stable-SAM, when provided with sub-optimal prompts. Our Stable-SAM consistently surpasses other methods across prompts of different quality, demonstrating better or comparable performance to the SAM prompted by ground truth box. The bottom row displays the predicted masks and sampled important image features of SAM and Stable-SAM, with orange circles representing the attention weights, where a larger radius indicates a higher score. (a) SAM yields satisfactory segmentation results when provided with a high-quality box prompt. (b) Even a minor prompt modification leads to unstable segmentation output. SAM incorrectly segments the background, where the inaccurate box prompt misleads SAM to spend more attention to the background. (c) Our Stable-SAM accurately segments the target object by shifting more feature sampling attention to it.

its superior zero-shot generalization ability on new tasks and data distributions. Empowered by the billion-scale training masks and the promptable model design, SAM generalizes to various visual structures in diverse scenarios through flexible prompts, such as box, point, mask or text prompts. Facilitated by high-quality prompts, SAM has produced significant performance benefit for various impor-

Qi Fan (fanqics@gmail.com) done this work at Kuaishou Technology.
Xin Tao (jiangsutx@gmail.com) is the corresponding author.

tant applications, such as healthcare [26, 48], remote sensing [13, 61], self-driving [12, 17], agriculture [42, 50], *etc.*

Previous works mainly focus on improving SAM’s segmentation performance assuming high-quality prompts are available, such as a tight bounding box (*e.g.*, produced by SOTA detectors [29, 64, 68]) or sufficient points (*e.g.*, 10 points) for the target object. However, in practice SAM or in fact interactive segmentation often encounters inaccurate or insufficient prompts, casually marked up by users as inaccurate box or very sparse points, especially in the crowd-sourcing annotation platform. Such inaccurate prompts often mislead SAM to produce unstable segmentation results as shown in Figure 1. Unfortunately, however, this critical issue has been largely overlooked, even though the suboptimal prompts and the resulting segmentation stability problem are quite prevalent in practice.

Note that there is no proper off-the-shelf solution for solving SAM’s segmentation stability problem with inaccurate prompts. Simply finetuning SAM’s mask decoder with imprecise prompts may easily lead to catastrophic forgetting, undermining the integrity of the highly-optimized SAM model and thus sacrificing the zero-shot segmentation generality. Although in the image domain deformable attention [10, 63] has shown impressive efficacy on adaptively shifting the model attention to informative regions, which may naturally address the attention drift issue caused by the misleading prompts, a straightforward implementation of this idea can again compromise SAM’s integrity.

In this paper we present the first comprehensive analysis on SAM’s segmentation stability across a wide range of prompt qualities, with a particular focus on low-quality prompts such as imprecise bounding boxes or points. Our findings demonstrate that, when fed with imprecise prompts, the SAM’s mask decoder is likely to be misguided to focus on the background or specific object parts, where the cross-attention module is inclined to aggregate and activate image features of these regions when mutually updating the prompt and image tokens. Such collaborative token updating mechanism usually suffers from attention drift, which is accumulated and propagated from the sub-optimal prompt to the unsatisfactory segmentation results.

To address this issue, we present a novel deformable sampling plugin (DSP) with *two* key designs to improve SAM’s stability while maintaining its zero-shot generality. Our key idea is to adaptively adjust only the feature sampling locations for the whole image feature map, while keeping the original SAM model unchanged: 1) we employ a small offset network to predict the corresponding offsets for each image feature sampling locations, which are learned from the input image feature map; 2) then, we resample the deformable image features at the updated sampling locations for keys and values of the cross-attention module in SAM’s mask decoder, keeping the original SAM

model unchanged. In doing so, we can shift the feature sampling attention toward informative regions which is more likely to contain target objects, and meanwhile avoiding the potential model disruption of the original highly-optimized SAM. Finally, to effectively handle both the high- and low-quality prompts, we propose a dynamic routing module to toggle SAM between deformable and regular grid sampling modes. A simple and effective robust training strategy is proposed to facilitate our Stable-SAM to adapt to prompts of diverse qualities.

Thus, our method is unique in its idea and design on solely adjusting the feature sampling locations without involving the original model parameters. In contrast, the conventional deformable attention methods [10, 63] updates the original network parameters, which is undesirable when adapting powerful foundation models, especially when fine-tuning large foundation models. Our method thus improves SAM’s segmentation stability across a wide range of prompt qualities with minimal learnable parameters and fast adaptation, and meanwhile retains SAM’s powerful promptable segmentation efficiency and generality.

2. Related Works

Improving Segmentation Quality. Researchers have proposed various methods to enhance the quality and accuracy of semantic segmentation methods. Early methods incorporate graphical models such as CRF [36] or region growing [11] as an additional post-processing stage, which are usually training-free. Many learning-based methods design new operators [30, 31, 34] or utilize additional refinement stage [8, 55]. Recently, methods such as Mask2Former [7] and SAM [35] have been introduced, which address open-world segmentation by introducing prompt-based approaches. Along this line, a series of improvements [32, 38] have been proposed, focusing on prompt-tuning and improving the accuracy of segmentation decoders. However, these methods overlook a crucial aspect, which is how to generate high-quality segmentation results in cases where the prompt is inaccurate. This is precisely the problem that our method aims to address.

Tuning Foundation Models. Pretrained models have played an important role since the very beginning of deep learning [22, 37, 57]. Despite zero-shot generalization grows popular in foundation models of computer vision and natural language processing [4, 5], tuning methods such as adapter [25] and prompt-based learning [24, 25] have been proposed to generalize these models to downstream tasks [15, 16]. These methods typically involves additional training parameters and time. We propose a new method that makes better use of existing features with minimal additional methods and can also produce competitive results.

Deformable Attention. Deformable convolution [10, 69] has been proved effective to help neural features attend to

important spatial locations. Recently, it has also been extended to transformer-based networks [6, 63, 66, 70]. Such deformed spatial tokens are especially suitable for our task, which requires dynamically attending to correct regions given inaccurate prompts. However, previous deformable layers involve both offset learning and feature learning after deformation. In this paper, we propose a new approach by simply sampling and reusing the features using deformable operations, without the need to train subsequent layers.

3. SAM Stability Analysis

In this section, we present a comprehensive investigation into the stability of SAM under prompts of varying quality.

3.1. Segmentation Stability Metric

Prior segmentation studies have focused on achieving high prediction accuracy, gauged by the Intersection-over-Union (IoU) between the predicted and ground truth masks. This focus on high performance is justified as segmentation models typically produce deterministic masks for given input images, without requiring additional inputs.

However, SAM’s segmentation output depends on both the image and the prompts, with the latter often varying in quality due to different manual or automatic prompt generators. In practical applications of SAM, segmentation targets are typically clear and unambiguous, independent of prompt quality. For instance, in autonomous driving applications, the goal is to segment the entire car stably and consistently, regardless of whether the prompt—be it a point or a bounding box—initially focuses on a specific part such as the wheel or the car body.

Motivated by this application requirement, we introduce the segmentation stability metric. Specifically, SAM is capable of producing a set of binary segmentation maps $M \in \mathcal{R}^{B \times H \times W}$ for a single target object using B prompts of differing qualities. We define the segmentation stability (mSF) within the set as:

$$S = \frac{1}{B} \sum_{i=1}^B \text{IoU}(M_i, M_{\text{union}}), \quad (1)$$

where $\text{IoU}(M_i, M_{\text{union}})$ represents the Intersection-over-Union between the i -th segmentation map M_i and the collective foreground region $\bigcup_i^B M_i$ of all maps. This new metric assesses the consistency across segmentations in each prediction, serving as a reliable indicator of stability, even without access to the ground truth masks.

3.2. SAM Segmentation Instability

We perform empirical studies to illustrate the segmentation instability of the current SAM with prompts of differing quality, thereby justifying our Stable SAM approach.

Model and Evaluation Details. The released SAM is trained with crafted prompts on large-scale SA-1B dataset.



Figure 2. SAM performs badly when dealing with suboptimal prompts. This is mainly caused by the undesirable feature attention, focusing on the background or specific object parts. (The important features are highlighted by the orange circles, with larger radius indicating higher attention score. Please zoom-in on color screen for better visualization.)

Metric	GT Box	Noisy Box	1 Point	3 Points	5 Points	10 Points
mIoU	79.5	48.8	43.3	78.7	83.3	84.8
mBIOU	71.1	42.1	37.4	69.5	74.2	76.0
mSF	-	39.5	45.1	79.3	84.7	87.5

Table 1. SAM’s segmentation accuracy and stability under prompts of varying quality.

We evaluate the segmentation accuracy and stability of the ViT-Large based SAM with different prompt types and qualities, including box prompts with added noise (noise scale 0.4) and point prompts with varying numbers of points (1, 3, 5, 10 positive points randomly selected from the ground truth mask). For every input image and prompt type, we randomly select 20 prompts to compute their segmentation stability, average mask mIoU, and boundary mBIOU scores. The evaluation utilizes four segmentation datasets as in HQ-SAM [32]: DIS [51] (validation set), ThinObject5K [40] (test set), COIFT [46], and HR-SOD [67].

Table 1 tabulates that SAM’s segmentation accuracy and stability significantly decrease with low-quality prompts, such as imprecise box prompts or point prompts with minimal points. These analysis are performed on the four aforementioned segmentation datasets. The varying segmentation accuracy and stability indicates that SAM’s mask decoder performs distinctly when dealing with prompts of varying qualities.

We visualize the image activation map for the token-to-image cross-attention in SAM’s second mask decoder layer to better understand its response to low-quality prompts. We focus on the second mask decoder layer for visualization because its cross-attention is more representative, benefiting from the input tokens and image embedding collaboratively updated by the first mask decoder layer. Figure 2

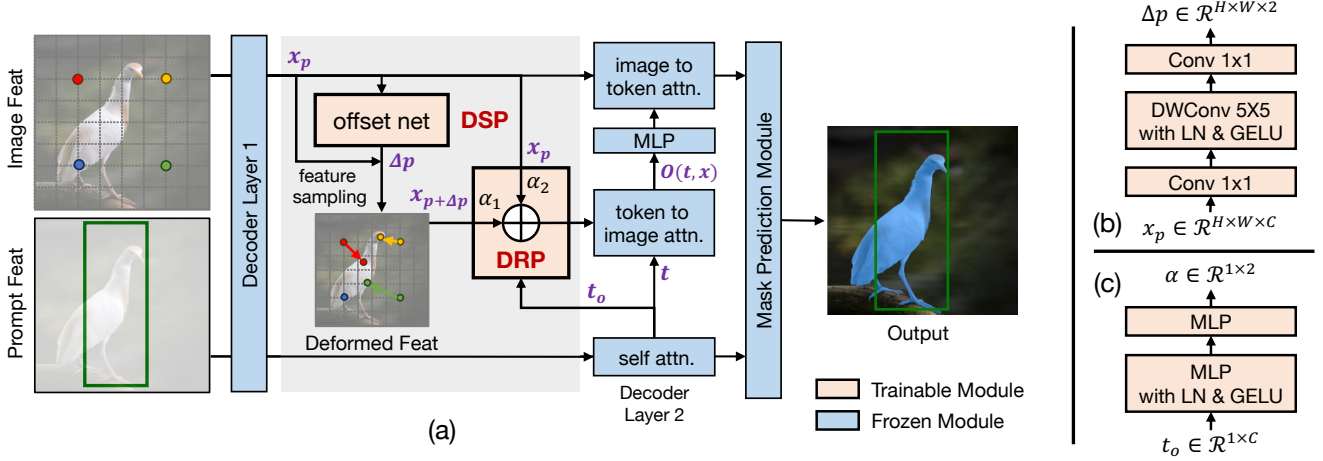


Figure 3. (a) An illustration of our deformable sampling plugin (DSP) and deformable routing plugin (DRP) in SAM’s mask decoder transformer. DSP employs a small (b) offset network to predict the feature sampling offset. Subsequently, DSP resamples deformable image features at the updated sampling locations and feeds them into SAM’s token-to-image attention. DRP employs a small (c) MLP network to regulate the degree of DSP activation based on the input prompt quality. Note that our DSP adaptively adjusts solely the image feature sampling locations without altering the original SAM model.

demonstrates that an inaccurate box prompt causes SAM’s mask decoder to miss regions of the target object while incorrectly incorporating features from the background, or focusing on specific object parts. It consequently leads to degraded segmentation accuracy and stability.

Overall, the above empirical evidence suggests that SAM potentially suffers from the attention drift issue, where suboptimal prompts misleadingly shift attention from the target object to background areas or specific object parts, thereby compromising the accuracy and stability of the segmentation results. This motivates us to calibrate SAM’s mask attention by leveraging learnable offsets to adjust the attention sampling position towards the target object regions, thus boosting segmentation accuracy and stability.

4. Stable Segment Anything Model

4.1. Preliminaries

We first revisit the recent Segment Anything Model (SAM) and deformable attention mechanism.

Segment Anything Model. SAM [35] is a powerful promptable segmentation model. It comprises an image encoder for computing image embeddings, a prompt encoder for embedding prompts, and a lightweight mask decoder for predicting segmentation masks by combining the two information sources. The fast mask mask decoder is a two-layer transformer-based decoder to collaboratively update both the image embedding and prompt tokens via cross-attention. SAM is trained on the large-scale SA-1B dataset.

Deformable Attention. Deformable attention [63] is a mechanism that enables the model to focus on a subset of key sampling points instead of the entire feature space. This mechanism naturally addresses the attention shift problem

in SAM caused by low-quality prompts.

In the standard self-attention, given a feature map $x \in \mathcal{R}^{H \times W \times C}$, the attention weights are computed across all spatial locations within the feature map.

In the deformable attention [63], a uniform grid of points $r \in \mathcal{R}^{H_G \times W_G \times 2}$ are first generated as the references¹ with the sampled image feature $x_r \in \mathcal{R}^{H_G \times W_G \times C}$. Subsequently, a convolutional offset network θ_{offset} predicts the offset $\Delta r = \theta_{\text{offset}}(x_r)$ for each reference point. The new feature sampling locations are given by $r + \Delta r \in \mathcal{R}^{H_G \times W_G \times 2}$. The resampled deformable image features $x_{r+\Delta r} \in \mathcal{R}^{H_G \times W_G \times C}$ are then utilized as the key and value features in the attention module.

Note that conventional deformable attention optimizes both the offset network and attention module. Thus directly applying deformable attention to SAM is usually suboptimal, because altering SAM’s original network or weights, e.g., substituting SAM’s standard attention with deformable attention and retraining, may compromise its integrity.

4.2. Deformable Sampling Plugin

To address the attention drift issue while preserving the SAM’s integrity, we propose a novel deformable sampling plugin (DSP) module on top of SAM’s original token-to-image cross-attention module, as shown in Figure 3.

Specifically, given the prompt token feature $t \in \mathcal{R}^{T \times C}$ and image feature $x_p \in \mathcal{R}^{H \times W \times C}$, the token-to-image cross-attention is:

$$\text{CAtn}(t, x) = \sigma(Q(t) \cdot K(x_p)^T) \cdot V(x_p), \quad (2)$$

where $p \in \mathcal{R}^{H \times W \times 2}$ represents the image feature spatial

¹With the grid size downsampled from the input feature map spatial size (H, W) by a factor of s , thus $H_G = H/s$ and $W_G = W/s$.

sampling locations, σ denotes the softmax function, and Q, K, V are the query, key, and value embedding projection functions, respectively

Our DSP adaptively adjusts solely the image feature sampling locations without altering the original SAM model. Specifically, we utilize an offset network θ_{offset} to predict the feature sampling offset $\Delta p \in \mathcal{R}^{H \times W \times 2}$, akin to that in deformable attention:

$$\Delta p = \theta_s(\theta_{\text{offset}}(x_p)), \quad (3)$$

where θ_s is a scale function $s_p \cdot \tanh(*)$ to prevent too large offset, and s_p is a pre-defined scale factor. The offset network θ_{offset} consists of a 1×1 convolution, a 5×5 depthwise convolution with the layer normalization and GELU activation, and a 1×1 convolution. The updated feature sampling locations are $p + \Delta p$. The numerical range of both p and $p + \Delta p$ lies in $\{(0, 0), \dots, (H - 1, W - 1)\}$, which is then normalized to the range $[-1, 1]$ for feature sampling.

Subsequently, we resample deformable image features $x_{p+\Delta p} \in \mathcal{R}^{H \times W \times C}$ at the updated sampling locations $p + \Delta p$ for keys and values. Thus, our DSP updates the token-to-image cross-attention of SAM’s mask decoder as:

$$\text{DCAttn}(t, x) = \sigma(Q(t) \cdot K(x_{p+\Delta p})^T) \cdot V(x_{p+\Delta p}). \quad (4)$$

As $p + \Delta p$ is fractional, we apply a bilinear interpolation to compute $x_{p+\Delta p}$ as in Deformable DETR [70].

Note that our DSP only trains the deformable offset network to predict new feature sampling locations $p + \Delta p$, and feeds the resampled deformable features $x_{p+\Delta p}$ to SAM’s cross-attention module. Thus, the original SAM model remains unchanged.

4.3. Dynamic Routing Plugin

While our DSP can effectively handle suboptimal and even erroneous prompts, by redirecting SAM’s attention to informative regions which are more likely to contain the target objects, high-quality prompts can typically direct the model’s attention correctly to target regions. Thus, it is essential to properly control the DSP’s activation to prevent unwanted attention shifts.

To address this issue, we propose a novel dynamic routing plugin (DRP) that regulates the degree of DSP activation based on the input prompt quality. The DRP can be formulated as follows:

$$\alpha = \sigma(\text{MLP}(t_o)) \cdot s, \quad (5)$$

where $t_o \in \mathbb{R}^{1 \times C}$ is the prompt token feature corresponding to the output mask, MLP refers to a small MLP network that includes an MLP layer with LayerNorm and GELU activation, as well as an output MLP layer; s denotes a learnable scale and σ denotes the softmax function.

We utilize the predicted values of $\alpha = [\alpha_1, \alpha_2] \in \mathbb{R}^{1 \times 2}$ to adaptively route SAM between DSP and original SAM’s

attention mechanism. Consequently, the token-to-image cross-attention output $O(t, x)$ can be formulated as:

$$O(t, x) = \text{CAttn}(t, \alpha_1 \cdot x_{p+\Delta p} + \alpha_2 \cdot x_p) \quad (6)$$

This soft dynamic routing strategy allows SAM to benefit from both DSP and its original zero-shot generality, contingent upon the quality of the prompt.

4.4. Robust Training Strategy

We propose a simple and effective robust training strategy (RTS) to assist our model to learn how to correct SAM’s attention when adversely affected by bad prompts.

Robust Training Against Inaccurate Prompts. SAM’s training, including HQ-SAM [32], typically utilizes high-quality prompts given by precise bounding boxes or multiple points to accurately identify the target object. To address inaccurate prompts, our RTS incorporates prompts of varying qualities during training. These prompts include groundtruth boxes, box prompts with added noise (noise scale 0.4), and point prompts with varying numbers of points (1, 3, 10 positive points randomly chosen from the ground truth mask).

Robust Training Against Ambiguous Prompts. In real segmentation scenarios, target objects often occur in cluttered environment, either occluding others or being occluded. Even given an accurate, tight bounding box, objects other than the target object will be enclosed. On the other hand, target objects are typically unambiguous even other objects are enclosed. For instance, in MS COCO, beds (occluded by quilt) are consistently regarded as target objects; the model must accurately segment the entire bed including accessories such as pillows and bedding. Thus, SAM’s original ambiguity-aware solution, which predicts *multiple* masks for a single prompt, is generally suboptimal in well-defined realistic applications. To address such “ambiguous” prompts, our RTS incorporates synthetic occlusion images to make SAM conducive to accurately segment target objects. The occlusion images are synthesized by randomly introducing other objects to simulate “occluder” and “occludee” relationship.

Our RTS is general and applicable to various SAM variants to improve their segmentation stability. Notably, our Stable-SAM with DSP and DRP experience the most substantial improvements from the application of RTS.

5. Experiments

Datasets. For fair comparison we keep our training and testing datasets same as HQ-SAM [32]. Specifically, we train all models on HQSeg-44K dataset, and evaluate their performance on four fine-grained segmentation datasets, including DIS [51] (validation set), ThinObject-5K [40] (test set), COIFT [46] and HR-SOD [67]. Furthermore,

Model	Epoch	Noisy Box			1 Point			3 Points		
		mIoU	mBIoU	mSF	mIoU	mBIoU	mSF	mIoU	mBIoU	mSF
SAM (baseline)	-	48.8	42.1	39.5	43.3	37.4	45.1	78.7	69.5	79.3
DT-SAM	12	70.6	60.4	64.0	43.1	43.2	37.9	80.3	71.6	80.5
PT-SAM	12	70.8	60.2	64.1	43.0	42.9	38.3	80.1	71.8	80.4
HQ-SAM [32]	12	72.4	62.8	65.5	43.2	44.6	37.4	81.8	73.7	81.4
Stable-SAM	1	82.3	74.1	82.3	76.9	68.4	71.1	84.0	75.8	84.9

Table 2. Comparison on four HQ datasets among SAM, DT-SAM (finetuning SAM’s mask decoder), PT-SAM (finetuning SAM’s prompt token and its corresponding output MLP layer), HQ-SAM and our Stable-SAM, under prompts of varying quality.

		MS COCO				SGinW					
Model	Epoch	N-Box (0.5-0.6)		N-Box (0.6-0.7)		N-Box (0.5-0.6)		N-Box (0.6-0.7)		Learnable Params	FPS
		mAP	mAP ₅₀	mAP	mAP ₅₀	mAP	mAP ₅₀	mAP	mAP ₅₀		
SAM (baseline)	-	27.3	60.2	40.9	75.0	26.0	60.8	39.5	73.2	(1191 M)	5.0
DT-SAM	12	12.2	22.7	15.8	28.7	10.4	21.5	13.6	27.1	3.9 M	5.0
PT-SAM	12	30.2	63.4	41.3	76.5	32.1	66.4	41.1	74.3	0.13 M	5.0
HQ-SAM [32]	12	31.9	65.5	42.9	77.1	33.6	68.4	42.2	75.9	5.1 M	4.8
Stable-SAM	1	44.8	76.4	50.5	81.1	43.3	75.6	48.6	79.4	0.08 M	5.0

Table 3. Comparison on MS COCO and SGinW datasets. All models are prompted by noisy boxes (N-Box) that overlap with the ground truth boxes, with IoU ranges of 0.5-0.6 and 0.6-0.7.

we validate the model’s zero-shot generalization ability on two challenging segmentation benchmarks, including COCO [41], and SGinW [71], where SGinW contains 25 zero-shot in-the-wild segmentation datasets. More experimental results are included in the supplementary material.

Input Prompts. We evaluate model’s accuracy and stability with prompts of differing type and quality, as described in Sec. 3.2. For MS COCO and SGinW, we do not use the boxes generated by SOTA detectors [29, 68] as the box prompt. This is because their predicted boxes are typically of high quality and cannot effectively evaluate the model’s segmentation stability in the presence of inaccurate boxes. Instead, we introduce random scale noises into the ground truth boxes to generate noisy boxes as the prompts. Specifically, to simulate inaccurate boxes while still having some overlap with the target object, we select noisy boxes that partially overlap with the ground truth boxes with IoU ranges of 0.5–0.6 and 0.6–0.7. We also evaluate our method using the box prompts generated by SOTA detectors.

Evaluation Metrics. We select suitable evaluation metrics depending on testing datasets, *i.e.*, 1) mask mIoU, boundary mBIoU and mSF for DIS, ThinObject-5K, COIFT, and HR-SOD; 2) mask mAP and mAP₅₀ for COCO and SGinW.

5.1. Comparison with SAM Variants

We compare our method with SAM and three powerful SAM variants. HQ-SAM is a recent powerful SAM variant for producing high-quality masks. We also try two simple SAM variants by finetuning its mask decoder and the

prompt token, *i.e.*, DT-SAM and PT-SAM, respectively. All our Stable-SAM models are trained by just one epoch for fast adaptation unless otherwise stated.

Stability Comparison on Four HQ Datasets. Table 2 shows the segmentation accuracy and stability on four HQ datasets, when models are fed with suboptimal prompts. Notably, the use of noisy box prompts significantly reduces SAM’s performance, as evidenced by the drop from 79.5/71.1 (as shown in Table 1) to 48.8/42.1 mIoU/mBIoU, accompanied by a low stability score of 39.5 mSF. This is probably because SAM was trained with solely high-quality prompts, thus seriously suffers from the low-quality prompts during inference. The other three SAM variants, namely HQ-SAM, DT-SAM, and PT-SAM, demonstrate relatively better stability in dealing with noisy boxes, which can be attributed to their long-term training on the HQSeg-44K dataset. Note our Stable-SAM can effectively address inaccurate box prompts, by enabling models to shifts attention to target objects. Given a single-point prompt, both SAM and its variants exhibit the lowest accuracy and stability. This indicates they are adversely affected by the ambiguity problem arising from the use of a single-point prompt. Although, in most practical applications, users prefer minimal interaction with clear and consistent segmentation targets. Our method maintains much better performance and stability when handling ambiguous one-point prompt, owing to our deformable feature sampling and robust training strategy against ambiguity. When point prompts increase to 3, all methods performs much better, while other methods



Figure 4. Visual results for box prompts (1st and 2nd row), for 1-point prompt (3rd) and 3-points prompt (4th). Within each image group in the first two rows, the three figures represent the results of SAM with GT box prompt, SAM with noisy box prompt, and Stable-SAM with noisy box prompt, respectively. The last two rows display the results of SAM and Stable-SAM with point prompts.

still under-perform compared with ours.

Generalization Comparison on MS COCO and SGenW.

Table 3 presents the segmentation accuracy and stability when the models are generalized to MS COCO and SGenW with noisy box prompts. Note that the DT-SAM performs the worst, probably due to overfitting on the training set, which compromises its ability to generalize to new datasets. Our method consistently surpasses all competitors, particularly in handling inaccurate boxes (N-Box 0.5–0.6), where all noisy boxes have an IoU range of 0.5–0.6 with the ground truth boxes. Note that our method has a minimal number of extra learnable parameters (0.08M) and can be quickly adapted to new datasets by just one training epoch.

Comparison Based on Detector Predicted Box Prompts.

Existing zero-shot segmentation methods typically choose powerful object detection model to generate high-quality boxes as the input prompts, such as FocalNet-L-DINO [64, 68]. We also evaluate our method in such setting. Table 4 presents that our model achieves comparable performance as SAM and PT-SAM when using the FocalNet-L-DINO generated high-quality boxes as prompts. When using the R50-H-Deformable-DETR [70] as the box prompt generator, our method achieves comparable performance as HQ-SAM. Note that training and implementing SOTA detectors typically require large computational resources and the cross-domain generalization is still very challenging. In practice, users tend to leverage interactive tools to annotate objects for their personalized datasets. Our method substantially surpasses other competitors in such scenario, when

Model	FocalNet-L-DINO		R50-H-D-DETR		Noisy Box	
	mAP	mAP ₅₀	mAP	mAP ₅₀	mAP	mAP ₅₀
SAM	48.5	75.3	41.5	63.7	27.3	60.2
PT-SAM	48.6	75.5	41.7	64.2	30.2	63.4
HQ-SAM	49.5	75.7	42.4	64.5	31.9	65.5
Ours	48.3	74.8	42.2	64.0	44.8	76.4

Table 4. Comparison on MS COCO with the box prompts generated by SOTA detectors or noisy box prompts.

the box can roughly indicate the target object.

5.2. Analysis on Stable-SAM

Deformable Sampling Plugin. Table 5 shows DSP can be trained with high-quality prompts (without RTS) to improve the performance and stability on low-quality prompts, although the model still exhibits some instability. When equipped with RTS, DSP can effectively learn to shift SAM’s attention to target objects when subjecting to inaccurate prompts. To delve deeper into the deformable sampling mechanism, we visualize the sampled feature points and their corresponding attention weights. Figure 4 illustrates how our DSP effectively shifts model’s attention to the target object, resulting in increased attention weights. Consequently, the cross-attention module aggregates more target object features into the prompt tokens, thereby improving the segmentation quality of the target objects.

Dynamic Routing Plugin. We leverage DSP to dynamically route the model between the regular and deformable

Model	Noisy Box			1 Point		
	mIoU	mBIOU	mSF	mIoU	mBIOU	mSF
SAM (baseine)	48.8	42.1	39.5	43.3	37.4	45.1
+ DSP	69.9	60.2	67.2	46.8	40.8	48.0
+ DSP + RTS	81.7	73.5	81.6	75.9	67.5	70.6
+ DSP + DRP + RTS	82.3	74.1	82.3	76.9	68.4	71.1

Table 5. Ablation study on deformable sampling plugin (DSP), dynamic routing plugin (DRP) and robust training strategy (RTS).

feature sampling modes, conditioned on the input prompt quality. We find that DRP tends to route more DSP features when dealing with worse prompts. The DSP routing weight α_1 is increased from 0.469 to 0.614 when we change the point prompt from three points to one point. It indicates that lower-quality prompts rely more on DSP features to shift attention to the desirable regions. Table 5 shows that DRP can further improve model’s performance, especially when handling the challenging one-point prompt scenario.

Robust Training Strategy. Robust training is critical for improving model’s segmentation stability, but is usually overlooked in previous works. RTS can guide the model, including our DSP, to accurately segment target objects even when provided with misleading low-quality prompts. Table 6 shows that RTS substantially improves the segmentation stability of all the methods, albeit with a slight compromise in performance when dealing with high-quality prompts. Note that our Stable-SAM benefits the most from the application of RTS, which can be attributed to our carefully designed deformable sampling plugin design.

Model Scalability. Our method solely adjusts model’s feature sampling locations using a minimal number of learnable parameters (0.08 M), while keeping the model architecture and parameters intact. This plugin design grants our method with excellent model scalability. Table 6 shows that our model can be rapidly optimized by just one training epoch, achieving comparable performance and stability. By scaling the training procedure to 12 epochs, our method achieves the best performance across all prompting settings. Additionally, our method can cooperate with other SAM variants. For instance, when combined with HQ-SAM, the performance and stability are further improved.

Low-Shot Generalization. Customized datasets with mask annotation are often limited, typically consisting of only hundreds of images. For a fair comparison, all methods in Table 7 are trained with RTS by 12 training epochs. Table 7 shows that HQ-SAM performs worst when trained with a limited number of images (220 or 440 images), which can be attributed to its potential overfitting problem caused by the relatively large learnable model parameters (5.1 M). In contrast, PT-SAM’s better performance with minimal learnable parameters (0.13 M) further validates this hypothesis. Our plugin design, coupled with minimal learnable param-

Model	Groundtruth Box		Noisy Box		
	mIoU	mBIOU	mIoU	mBIOU	mSF
SAM (baseine)	79.5	71.1	48.8	42.1	39.5
<i>Without RTS:</i>					
PT-SAM	87.6	79.7	70.6	60.4	64.0
HQ-SAM	89.1	81.8	72.4	62.8	65.5
Ours (1 epoch)	87.4	80.0	69.6	60.0	66.5
Ours (12 epochs)	89.1	82.1	72.7	63.2	67.4
<i>With RTS:</i>					
PT-SAM	86.8	78.4	82.1	73.1	78.7
HQ-SAM	87.4	79.8	82.9	74.5	80.4
Ours (1 epoch)	86.0	78.4	82.3	74.1	82.3
Ours (12 epochs)	87.4	80.1	84.4	76.7	85.2
HQ-SAM + Ours	88.7	81.5	86.1	78.7	86.3

Table 6. Model scalability study.

Model	Noisy Box			1 Point		
	mIoU	mBIOU	mSF	mIoU	mBIOU	mSF
SAM (baseine)	48.8	42.1	39.5	43.3	37.4	45.1
<i>220 train images:</i>						
PT-SAM	77.6	67.7	72.6	71.8	63.2	73.0
HQ-SAM	73.5	62.3	67.7	71.3	62.6	72.4
Ours	78.8	70.0	78.9	73.0	64.7	74.5
<i>440 train images:</i>						
PT-SAM	78.6	69.0	74.4	76.2	67.4	75.0
HQ-SAM	77.4	67.1	75.6	74.6	64.6	71.9
Ours	81.6	73.5	82.6	79.8	71.5	82.5

Table 7. Low-shot generalization comparison. All models are trained with RTS by 12 training epochs.

eters, enables effective low-shot generalization, and thus achieves the best performance in such scenario.

6. Conclusion

In this paper, we present the first comprehensive analysis on SAM’s segmentation stability across a wide range of prompt qualities. Our findings reveal that SAM’s mask decoder tends to activate image features that are biased to the background or specific object parts. We propose the novel Stable-SAM to address this issue by adjusting the sampling locations of image feature using learnable deformable offsets, while keeping the original SAM model unchanged. The deformable sampling plugin (DSP) allows SAM to adaptively shift attention to the prompted target regions in a data-driven manner. The dynamic routing plugin (DRP) toggles SAM between deformable and regular grid sampling modes depending on the quality of the input prompts. Our robust training strategy (RTS) facilitates Stable-SAM to effectively adapt to prompts of varying qualities. Extensive experiments on multiple datasets validate the effectiveness and advantages of our Stable-SAM.

Appendix

7. More Experimental Results

7.1. MESS

The recently released Multi-domain Evaluation of Semantic Segmentation (MESS) [3] is a large-scale benchmark for holistic analysis of zero-shot segmentation performance. MESS consists of 22 downstream tasks, a total of 448 classes, and 25079 images, covering a wide range of domain-specific datasets in the fields of earth monitoring, medical sciences, engineering, agriculture and biology and other general domains. We evaluate SAM [35], HQ-SAM [32] and our Stable-SAM on MESS benchmark using the official MESS evaluation code, and report the mean of class-wise intersection over union (mIoU).

Following MESS’s model settings, our Stable-SAM selects the first mask of the predicted multiple masks as the output. For a fair comparison, our Stable-SAM follows HQ-SAM to fuse the SAM’s original prediction map into our predicted segmentation map. We provide four prompt types for evaluation. The *oracle point* refers to a single point sampled from the ground-truth mask using the point sampling approach RITM [58]. The *random point* refers to a single point randomly sampled from the ground-truth mask of the target object. The *oracle box* refers to a single box tightly enclosing the ground-truth mask of the target object. The *noisy box* refers to a single box generated by adding noise (noise scale 0.4) to the *oracle box*.

Table 8 tabulates the zero-shot semantic segmentation performance comparison on MESS. Our Stable-SAM performs best when prompted with *oracle point*, *random point* and *noisy box*, and achieves comparable performance when

provided with *oracle box*. Our competitive performance on the large-scale MESS benchmark further consolidates the powerful zero-shot generalization ability inherent in our Stable-SAM. Table 9 shows the dataset and comparison details on 22 tasks of MESS benchmark. Our Stable-SAM performs best on 19 out of 22 datasets.

7.2. Backbone Variants

Table 10 tabulates the performance comparison on different backbone variants. Our Stable-SAM consistently performs better than other methods on all backbone variants.

8. Relation to Other Methods

Deformable Attention. Our method is unique in its idea and design on solely adjusting the feature sampling locations by training the offset network, without involving the original model parameters. In contrast, conventional deformable attention methods [10, 63] train both the offset network and original network parameters, which is undesirable when adapting powerful foundation models in deployment, especially in finetuning large foundation models. Figure 5 shows the difference between our deformable sampling plugin and conventional deformable attention.

We apply the conventional deformable attention in our Stable-SAM by finetuning the mask decoder during training. Table 11 shows that the conventional deformable attention (Stable-SAM (finetuning decoder)) exhibits the worst generalization ability on MS COCO, even worse than the original SAM model. This further validates the necessity and better performance of our deformable sampling plugin paradigm, *i.e.*, adapting the foundation model by only adjusting the feature sampling locations, while fixing the orig-

Model	Prompt	General	Earth Monitoring	Medical Sciences	Engineering	Agriculture & Biology	Mean
SAM	Oracle Point	46.51	42.31	55.92	51.57	57.43	49.67
HQ-SAM		44.05	40.82	61.0	54.18	53.92	49.58
Stable-SAM (Ours)		49.10	43.23	54.45	53.52	60.92	51.15
SAM	Oracle Box	77.85	73.03	64.89	73.03	86.75	74.74
HQ-SAM		76.63	68.03	65.1	74.78	85.34	73.43
Stable-SAM (Ours)		77.91	72.84	62.93	73.12	85.63	74.21
SAM	Random Point	40.21	36.74	53.20	47.15	49.75	44.34
HQ-SAM		38.81	36.62	58.27	51.43	44.51	44.92
Stable-SAM (Ours)		42.43	37.30	50.89	48.96	53.42	45.49
SAM	Noisy Box	55.97	55.12	62.45	62.34	64.26	59.24
HQ-SAM		52.02	47.15	62.57	62.02	60.56	55.81
Stable-SAM (Ours)		59.82	58.86	62.19	64.56	68.84	62.13

Table 8. Comparison on Multi-domain Evaluation of Semantic Segmentation (MESS) benchmark, consisting of 22 downstream datasets, 448 classes, and 25,079 images.

Dataset	Domain	Sensor type	Mask size	# Classes	# Images	Task	SAM	HQ	Ours
BDD100K [65]	General	Visible spectrum	Medium	19 (Medium)	1,000	Driving	48.9	43.66	51.84
Dark Zurich [53]		Visible spectrum	Medium	20 (Medium)	50	Driving	54.34	50.85	56.81
MHP v1 [39]		Visible spectrum	Small	19 (Medium)	980	Body parts	66.64	62.63	69.11
FoodSeg103 [20]		Visible spectrum	Medium	104 (Many)	2,135	Ingredients	57.98	56.22	64.12
ATLANTIS [14]		Visible spectrum	Small	56 (Many)	1,295	Maritime	56.23	48.7	60.04
DRAM [9]		Visible spectrum	Medium	12 (Medium)	718	Paintings	51.73	50.06	57.03
iSAID [59]	Earth Monitoring	Visible spectrum	Small	16 (Medium)	4,055	Objects	65.2	62.6	67.46
ISPRS Potsdam [33]		Multispectral	Small	6 (Few)	504	Land use	47.32	38.43	50.92
WorldFloods [47]		Multispectral	Medium	3 (Binary)	160	Floods	57.61	49.46	60.81
FloodNet [52]		Visible spectrum	Medium	10 (Few)	5,571	Floods	51.85	39.82	58.31
UAVid [44]		Visible spectrum	Small	8 (Few)	840	Objects	53.62	45.43	56.82
Kvasir-Inst. [28]	Medical Sciences	Visible spectrum	Medium	2 (Binary)	118	Endoscopy	83.62	81.32	85.87
CHASE DB1 [18]		Microscopic	Small	2 (Binary)	20	Retina scan	34.59	37.5	33.88
CryoNuSeg [45]		Microscopic	Small	2 (Binary)	30	WSI	72.87	72.78	73.09
PAXRay-4 [54]		Electromagnetic	Large	4x2 (Binary)	180	X-Ray	58.72	58.66	55.94
Corrosion CS [2]	Engineering	Visible spectrum	Medium	4 (Few)	44	Corrosion	53.05	51.86	55.47
DeepCrack [43]		Visible spectrum	Small	2 (Binary)	237	Cracks	56.36	60.84	58.2
ZeroWaste-f [1]		Visible spectrum	Medium	5 (Few)	929	Conveyor	70.23	69.52	74.01
PST900 [56]		Electromagnetic	Small	5 (Few)	288	Thermal	69.71	65.88	70.55
SUIM [27]	Agriculture & Biology	Visible spectrum	Medium	8 (Few)	110	Underwater	56.98	47.51	62.35
CUB-200 [60]		Visible spectrum	Medium	201 (Many)	5,794	Bird species	56.3	54.54	64.57
CWFID [21]		Visible spectrum	Small	3 (Few)	21	Crops	79.49	79.63	79.61
Mean IoU	–	–	–	–	–	–	59.24	55.81	62.13

Table 9. Dataset and comparison details on MESS benchmark. Models are prompted with noisy boxes. “HQ” denotes HQ-SAM.

		MS COCO		Four HQ Datasets									
Model	Epoch	N-Box (0.5-0.6) mAP	mAP ₅₀	Noisy Box mIoU	mBiou	mSF	1 Point mIoU	mBiou	mSF	Params (M) Total	Trainable	FPS	Mem.
SAM-Huge	-	25.6	56.8	50.1	43.2	40.4	44.5	38.3	46.5	2446	2446	3.5	10.3G
HQ-SAM-Huge	12	30.0	62.6	75.2	65.5	69.3	48.0	41.1	49.5	2452.1	6.1	3.4	10.3G
Stable-SAM-Huge	1	43.9	75.7	81.8	73.5	82.3	77.2	68.9	74.6	2446.08	0.08	3.5	10.3G
SAM-Large	-	27.3	60.2	48.8	42.1	39.5	43.3	37.4	45.1	1191	1191	5.0	7.6G
HQ-SAM-Large	12	31.9	65.5	72.4	62.8	65.5	43.2	44.6	37.4	1196.1	5.1	4.8	7.6G
Stable-SAM-Large	1	44.8	76.4	82.3	74.1	82.3	76.9	68.4	71.1	1191.08	0.08	5.0	7.6G
SAM-Base	-	19.7	49.2	41.6	35.8	33.4	35.1	29.2	36.7	358	358	10.1	5.1G
HQ-SAM-Base	12	24.7	56.1	68.7	59.1	63.2	40.6	35.7	42.7	362.1	4.1	9.8	5.1G
Stable-SAM-Base	1	31.2	63.3	74.7	64.8	75.9	68.9	59.5	67.1	358.08	0.08	10.1	5.1G

Table 10. Comparison on MS COCO and four HQ datasets for different backbone variants.

inal model features and parameters.

Spatial Attention. The spatial attention [23, 62] can adjust the image spatial feature weights, and thus can be regarded as a soft feature sampling method. We directly replace DSP with spatial attention in our Stable-SAM to investigate if spatial attention offers comparable effectiveness. Table 11

shows that spatial attention performs much worse than our DSP, although it consistently improves the segmentation performance and stability on all datasets. This indicates that simply adjusting the feature weights is insufficient to adapt SAM for handling suboptimal prompts.

	MS COCO		Four HQ Datasets					
Model	N-Box (0.5-0.6) mAP mAP ₅₀		Noisy Box mIoU mBLoU mSF			1 Point mIoU mBLoU mSF		
SAM	27.3	60.2	48.8	42.1	39.5	43.3	37.4	45.1
Stable-SAM (finetuning decoder)	25.7	56.5	78.5	69.2	79.9	76.0	67.1	78.2
Stable-SAM (spatial attention)	29.8	64.9	69.3	59.8	57.8	51.6	44.5	49.1
Stable-SAM	44.8	76.4	82.3	74.1	82.3	76.9	68.4	71.1

Table 11. Comparison on MS COCO and four HQ datasets for different Stable-SAM variants. The “finetuning decoder” denotes finetuning the mask decoder when training Stable-SAM.

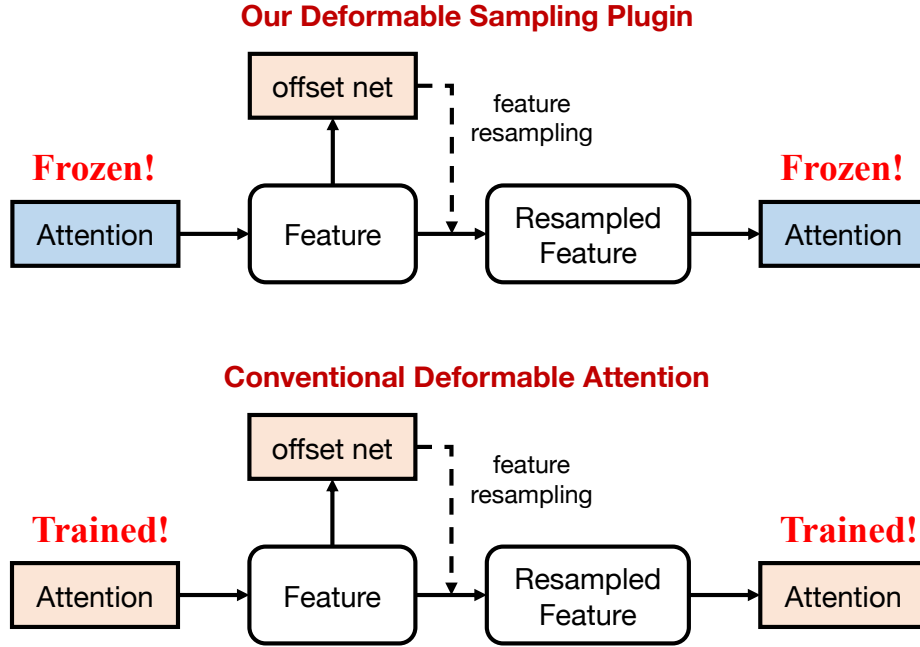


Figure 5. Method difference between our deformable sampling plugin and conventional deformable attention.

9. Implementation Details

During training, we only train DSP and DRP on HQSeg-44K dataset while fixing the model parameters of the pre-trained SAM model. We train Stable-SAM on 8 NVIDIA Tesla V100 GPUs with a total batch size of 32, using Adam optimizer with zero weight decay and 0.001 learning rate. The training images are augmented using large-scale jittering [19]. The input prompts are randomly sampled from mixed prompt types, including ground truth bounding boxes, randomly sampled points (1, 3, 5, 10 positive points randomly selected from the ground truth mask), noisy boxes (generated by adding noise (noise scale 0.4) to the ground truth bounding boxes, where we ensure the generated noisy boxes have at least 0.5 overlap IoU with the ground truth boxes), and coarse masks (generated by adding Gaussian noise in the boundary regions of the ground truth masks).

The model is optimized using cross entropy loss and dice loss [49].

We follow the same inference pipeline of the original SAM. The mask decoder first predicts a small mask in 256×256 spatial resolution for each prompt, which is then up-sampled to the original resolution 1024×1024 as the output mask.

10. Stability Visualization

Figure 6-16 show extensive visualization comparisons between SAM and Stable-SAM, under box, 3-points and 1-point prompts of diverse qualities. We also visualize the image activation map for the token-to-image cross-attention in SAM’s second mask decoder layer to better understand its response to low-quality prompts. The important features are highlighted by the orange circles, with larger radius

indicating higher attention score. SAM yields unsatisfactory segmentation results when provided with low-quality prompts, and even a minor prompt modification leads to unstable segmentation output. In contrast, our Stable-SAM produces consistent and accurate mask predictions even under prompts of diverse qualities, by shifting more feature sampling attention to the target object.

References

- [1] Dina Bashkirova, Mohamed Abdelfattah, Ziliang Zhu, James Akl, Fadi Alladkani, Ping Hu, Vitaly Ablavsky, Berk Calli, Sarah Adel Bargal, and Kate Saenko. Zerowaste dataset: towards deformable object segmentation in cluttered scenes. In *CVPR*, 2022. 10
- [2] Eric Bianchi and Matthew Hebdon. Corrosion condition state semantic segmentation dataset. *University Libraries, Virginia Tech: Blacksburg, VA, USA*, 2021. 10
- [3] Benedikt Blumenstiel, Johannes Jakubik, Hilde Kühne, and Michael Vössing. What a MESS: Multi-Domain Evaluation of Zero-shot Semantic Segmentation. In *NeurIPS Workshop*, 2023. 9
- [4] Rishi Bommasani, Drew A Hudson, Ehsan Adeli, Russ Altman, Simran Arora, Sydney von Arx, Michael S Bernstein, Jeannette Bohg, Antoine Bosselut, Emma Brunskill, et al. On the opportunities and risks of foundation models. *arXiv preprint arXiv:2108.07258*, 2021. 2
- [5] Tom Brown, Benjamin Mann, Nick Ryder, Melanie Subbiah, Jared D Kaplan, Prafulla Dhariwal, Arvind Neelakantan, Pranav Shyam, Girish Sastry, Amanda Askell, et al. Language models are few-shot learners. *NeurIPS*, 2020. 2
- [6] Zhiyang Chen, Yousong Zhu, Chaoyang Zhao, Guosheng Hu, Wei Zeng, Jinqiao Wang, and Ming Tang. Dpt: Deformable patch-based transformer for visual recognition. In *ACM MM*, 2021. 3
- [7] Bowen Cheng, Ishan Misra, Alexander G Schwing, Alexander Kirillov, and Rohit Girdhar. Masked-attention mask transformer for universal image segmentation. In *CVPR*, 2022. 2
- [8] Ho Kei Cheng, Jihoon Chung, Yu-Wing Tai, and Chi-Keung Tang. Cascadepnp: Toward class-agnostic and very high-resolution segmentation via global and local refinement. In *CVPR*, 2020. 2
- [9] Nadav Cohen, Yael Newman, and Ariel Shamir. Semantic segmentation in art paintings. In *Computer Graphics Forum*, 2022. 10
- [10] Jifeng Dai, Haozhi Qi, Yuwen Xiong, Yi Li, Guodong Zhang, Han Hu, and Yichen Wei. Deformable convolutional networks. In *ICCV*, 2017. 2, 9
- [11] Philippe Ambrozio Dias and Henry Medeiros. Semantic segmentation refinement by monte carlo region growing of high confidence detections. In *ACCV*, 2019. 2
- [12] Atharva Dikshit, Alison Bartsch, Abraham George, and Amir Barati Farimani. Robochop: Autonomous framework for fruit and vegetable chopping leveraging foundational models. *arXiv preprint arXiv:2307.13159*, 2023. 2
- [13] Lei Ding, Kun Zhu, Daifeng Peng, Hao Tang, and Haitao Guo. Adapting segment anything model for change detection in hr remote sensing images. *arXiv preprint arXiv:2309.01429*, 2023. 2
- [14] Seyed Mohammad Hassan Erfani, Zhenyao Wu, Xinyi Wu, Song Wang, and Erfan Goharian. Atlantis: A benchmark for semantic segmentation of waterbody images. *Environmental Modelling & Software*, 2022. 10
- [15] Qi Fan, Wei Zhuo, Chi-Keung Tang, and Yu-Wing Tai. Few-shot object detection with attention-rpn and multi-relation detector. In *CVPR*, 2020. 2
- [16] Qi Fan, Wenjie Pei, Yu-Wing Tai, and Chi-Keung Tang. Self-support few-shot semantic segmentation. In *ECCV*, 2022. 2
- [17] Qi Fan, Mattia Segu, Yu-Wing Tai, Fisher Yu, Chi-Keung Tang, Bernt Schiele, and Dengxin Dai. Towards robust object detection invariant to real-world domain shifts. In *ICLR*, 2022. 2
- [18] Muhammad Moazam Fraz, Paolo Remagnino, Andreas Hoppe, Bunyarit Uyyanonvara, Alicja R Rudnicka, Christopher G Owen, and Sarah A Barman. An ensemble classification-based approach applied to retinal blood vessel segmentation. *IEEE Transactions on Biomedical Engineering*, 2012. 10
- [19] Golnaz Ghiasi, Yin Cui, Aravind Srinivas, Rui Qian, Tsung-Yi Lin, Ekin D Cubuk, Quoc V Le, and Barret Zoph. Simple copy-paste is a strong data augmentation method for instance segmentation. In *CVPR*, 2021. 11
- [20] Rahul Ghosh, Praveen Ravirathinam, Xiaowei Jia, Ankush Khandelwal, David Mulla, and Vipin Kumar. Calcrop21: A georeferenced multi-spectral dataset of satellite imagery and crop labels. In *ICBD*, 2021. 10
- [21] Sebastian Haug and Jörn Ostermann. A crop/weed field image dataset for the evaluation of computer vision based precision agriculture tasks. In *ECCV Workshops*, 2015. 10
- [22] Kaiming He, Xiangyu Zhang, Shaoqing Ren, and Jian Sun. Deep residual learning for image recognition. In *CVPR*, 2016. 2
- [23] Qibin Hou, Daquan Zhou, and Jiashi Feng. Coordinate attention for efficient mobile network design. In *CVPR*, 2021. 10
- [24] Neil Houlsby, Andrei Giurgiu, Stanislaw Jastrzebski, Bruna Morrone, Quentin De Laroussilhe, Andrea Gesmundo, Mona Attariyan, and Sylvain Gelly. Parameter-efficient transfer learning for nlp. In *ICML*, 2019. 2
- [25] Edward J Hu, Yelong Shen, Phillip Wallis, Zeyuan Allen-Zhu, Yanzhi Li, Shean Wang, Lu Wang, and Weizhu Chen. Lora: Low-rank adaptation of large language models. In *ICLR*, 2022. 2
- [26] Yuhao Huang, Xin Yang, Lian Liu, Han Zhou, Ao Chang, Xinrui Zhou, Rusi Chen, Junxuan Yu, Jiongquan Chen, Chaoyu Chen, et al. Segment anything model for medical images? *arXiv preprint arXiv:2304.14660*, 2023. 2
- [27] Md Jahidul Islam, Chelsey Edge, Yuyang Xiao, Peigen Luo, Muntaqim Mehtaz, Christopher Morse, Sadman Sakib Enan, and Junaed Sattar. Semantic segmentation of underwater imagery: Dataset and benchmark. In *IROS*, 2020. 10

- [28] Debesh Jha, Sharib Ali, Krister Emanuelsen, Steven A Hicks, Vajira Thambawita, Enrique Garcia-Ceja, Michael A Riegler, Thomas de Lange, Peter T Schmidt, Håvard D Johansen, et al. Kvasir-instrument: Diagnostic and therapeutic tool segmentation dataset in gastrointestinal endoscopy. In *MultiMedia Modeling*, 2021. 10
- [29] Ding Jia, Yuhui Yuan, Haodi He, Xiaopei Wu, Haojun Yu, Weihong Lin, Lei Sun, Chao Zhang, and Han Hu. Detsr with hybrid matching. In *CVPR*, 2023. 2, 6
- [30] Lei Ke, Martin Danelljan, Xia Li, Yu-Wing Tai, Chi-Keung Tang, and Fisher Yu. Mask transfiner for high-quality instance segmentation. In *CVPR*, 2022. 2
- [31] Lei Ke, Henghui Ding, Martin Danelljan, Yu-Wing Tai, Chi-Keung Tang, and Fisher Yu. Video mask transfiner for high-quality video instance segmentation. In *ECCV*, 2022. 2
- [32] Lei Ke, Mingqiao Ye, Martin Danelljan, Yifan Liu, Yu-Wing Tai, Chi-Keung Tang, and Fisher Yu. Segment anything in high quality. In *NeurIPS*, 2023. 2, 3, 5, 6, 9
- [33] Kourosh Khoshelham, L Díaz Vilariño, Michael Peter, Zhizhong Kang, and Debaditya Acharya. The isprs benchmark on indoor modelling. *The International Archives of the Photogrammetry, Remote Sensing and Spatial Information Sciences*, 2017. 10
- [34] Alexander Kirillov, Yuxin Wu, Kaiming He, and Ross Girshick. Pointrend: Image segmentation as rendering. In *CVPR*, 2020. 2
- [35] Alexander Kirillov, Eric Mintun, Nikhila Ravi, Hanzi Mao, Chloe Rolland, Laura Gustafson, Tete Xiao, Spencer Whitehead, Alexander C. Berg, Wan-Yen Lo, Piotr Dollar, and Ross Girshick. Segment anything. In *ICCV*, 2023. 1, 2, 4, 9
- [36] Philipp Krähenbühl and Vladlen Koltun. Efficient inference in fully connected crfs with gaussian edge potentials. *NeurIPS*, 2011. 2
- [37] Alex Krizhevsky, Ilya Sutskever, and Geoffrey E Hinton. Imagenet classification with deep convolutional neural networks. *NeurIPS*, 2012. 2
- [38] Feng Li, Hao Zhang, Peize Sun, Xueyan Zou, Shilong Liu, Jianwei Yang, Chunyuan Li, Lei Zhang, and Jianfeng Gao. Semantic-sam: Segment and recognize anything at any granularity. *arXiv preprint arXiv:2307.04767*, 2023. 2
- [39] Jianshu Li, Jian Zhao, Yunchao Wei, Congyan Lang, Yidong Li, Terence Sim, Shuicheng Yan, and Jiashi Feng. Multiple-human parsing in the wild. *arXiv preprint arXiv:1705.07206*, 2017. 10
- [40] Jun Hao Liew, Scott Cohen, Brian Price, Long Mai, and Jiashi Feng. Deep interactive thin object selection. In *WACV*, 2021. 3, 5
- [41] Tsung-Yi Lin, Michael Maire, Serge Belongie, James Hays, Pietro Perona, Deva Ramanan, Piotr Dollár, and C Lawrence Zitnick. Microsoft coco: Common objects in context. *ECCV*, 2014. 6
- [42] Xuanyu Liu. A sam-based method for large-scale crop field boundary delineation. In *SECON*, 2023. 2
- [43] Yahui Liu, Jian Yao, Xiaohu Lu, Renping Xie, and Li Li. Deepcrack: A deep hierarchical feature learning architecture for crack segmentation. *Neurocomputing*, 2019. 10
- [44] Ye Lyu, George Vosselman, Gui-Song Xia, Alper Yilmaz, and Michael Ying Yang. Uavid: A semantic segmentation dataset for uav imagery. *ISPRS journal of photogrammetry and remote sensing*, 2020. 10
- [45] Amirreza Mahbod, Gerald Schaefer, Benjamin Bancher, Christine Löw, Georg Dorffner, Rupert Ecker, and Isabella Ellinger. Cryonuseg: A dataset for nuclei instance segmentation of cryosectioned h&e-stained histological images. *Computers in biology and medicine*, 2021. 10
- [46] Lucy Alsina Choque Mansilla and Paulo André Vechiatto de Miranda. Object segmentation by oriented image foresting transform with connectivity constraints. In *ICIP*, 2019. 3, 5
- [47] Gonzalo Mateo-Garcia, Joshua Veitch-Michaelis, Lewis Smith, Silviu Vlad Oprea, Guy Schumann, Yarin Gal, Atılım Güneş Baydin, and Dietmar Backes. Towards global flood mapping onboard low cost satellites with machine learning. *Scientific reports*, 2021. 10
- [48] Maciej A Mazurowski, Haoyu Dong, Hanxue Gu, Jichen Yang, Nicholas Konz, and Yixin Zhang. Segment anything model for medical image analysis: an experimental study. *Medical Image Analysis*, 2023. 2
- [49] Fausto Milletari, Nassir Navab, and Seyed-Ahmad Ahmadi. V-net: Fully convolutional neural networks for volumetric medical image segmentation. In *3DV*, 2016. 11
- [50] Khoa Dang Nguyen, Thanh-Hai Phung, and Hoang-Giang Cao. A sam-based solution for hierarchical panoptic segmentation of crops and weeds competition. In *ICCVW*, 2023. 2
- [51] Xuebin Qin, Hang Dai, Xiaobin Hu, Deng-Ping Fan, Ling Shao, and Luc Van Gool. Highly accurate dichotomous image segmentation. In *ECCV*, 2022. 3, 5
- [52] Maryam Rahnemoonfar, Tashnim Chowdhury, Argho Sarkar, Debvrat Varshney, Masoud Yari, and Robin Robertson Murphy. Floodnet: A high resolution aerial imagery dataset for post flood scene understanding. *IEEE Access*, 2021. 10
- [53] Christos Sakaridis, Dengxin Dai, and Luc Van Gool. Guided curriculum model adaptation and uncertainty-aware evaluation for semantic nighttime image segmentation. In *ICCV*, 2019. 10
- [54] Constantin Seibold, Simon Reiß, Saquib Sarfraz, Matthias A Fink, Victoria Mayer, Jan Sellner, Moon Sung Kim, Klaus H Maier-Hein, Jens Kleesiek, and Rainer Stiefelhagen. Detailed annotations of chest x-rays via ct projection for report understanding. In *BMVC*, 2022. 10
- [55] Tiancheng Shen, Yuechen Zhang, Lu Qi, Jason Kuen, Xingyu Xie, Jianlong Wu, Zhe Lin, and Jiaya Jia. High quality segmentation for ultra high-resolution images. In *CVPR*, 2022. 2
- [56] Shreyas S Shivakumar, Neil Rodrigues, Alex Zhou, Ian D Miller, Vijay Kumar, and Camillo J Taylor. Pst900: Rgb-thermal calibration, dataset and segmentation network. In *ICRA*, 2020. 10
- [57] Karen Simonyan and Andrew Zisserman. Very deep convolutional networks for large-scale image recognition. In *ICLR*, 2015. 2

- [58] Konstantin Sofiiuk, Ilya A Petrov, and Anton Konushin. Re-viving iterative training with mask guidance for interactive segmentation. In *ICIP*, 2022. 9
- [59] Syed Waqas Zamir, Aditya Arora, Akshita Gupta, Salman Khan, Guolei Sun, Fahad Shahbaz Khan, Fan Zhu, Ling Shao, Gui-Song Xia, and Xiang Bai. isaid: A large-scale dataset for instance segmentation in aerial images. In *CVPR Workshops*, 2019. 10
- [60] Peter Welinder, Steve Branson, Takeshi Mita, Catherine Wah, Florian Schroff, Serge Belongie, and Pietro Perona. Caltech-ucsd birds 200. 2010. 10
- [61] Congcong Wen, Yuan Hu, Xiang Li, Zhenghang Yuan, and Xiao Xiang Zhu. Vision-language models in remote sensing: Current progress and future trends. *arXiv preprint arXiv:2305.05726*, 2023. 2
- [62] Sanghyun Woo, Jongchan Park, Joon-Young Lee, and In So Kweon. Cbam: Convolutional block attention module. In *ECCV*, 2018. 10
- [63] Zhuofan Xia, Xuran Pan, Shiji Song, Li Erran Li, and Gao Huang. Vision transformer with deformable attention. In *CVPR*, 2022. 2, 3, 4, 9
- [64] Jianwei Yang, Chunyuan Li, Xiyang Dai, and Jianfeng Gao. Focal modulation networks. In *NeurIPS*, 2022. 2, 7
- [65] Fisher Yu, Haofeng Chen, Xin Wang, Wenqi Xian, Yingying Chen, Fangchen Liu, Vashisht Madhavan, and Trevor Darrell. Bdd100k: A diverse driving dataset for heterogeneous multitask learning. In *CVPR*, 2020. 10
- [66] Xiaoyu Yue, Shuyang Sun, Zhanghui Kuang, Meng Wei, Philip HS Torr, Wayne Zhang, and Dahua Lin. Vision transformer with progressive sampling. In *ICCV*, 2021. 3
- [67] Yi Zeng, Pingping Zhang, Jianming Zhang, Zhe Lin, and Huchuan Lu. Towards high-resolution salient object detection. In *ICCV*, 2019. 3, 5
- [68] Hao Zhang, Feng Li, Shilong Liu, Lei Zhang, Hang Su, Jun Zhu, Lionel Ni, and Heung-Yeung Shum. DINO: DETR with improved denoising anchor boxes for end-to-end object detection. In *ICLR*, 2023. 2, 6, 7
- [69] Xizhou Zhu, Han Hu, Stephen Lin, and Jifeng Dai. Deformable convnets v2: More deformable, better results. In *CVPR*, 2019. 2
- [70] Xizhou Zhu, Weijie Su, Lewei Lu, Bin Li, Xiaogang Wang, and Jifeng Dai. Deformable detr: Deformable transformers for end-to-end object detection. In *ICLR*, 2020. 3, 5, 7
- [71] Xueyan Zou, Zi-Yi Dou, Jianwei Yang, Zhe Gan, Linjie Li, Chunyuan Li, Xiyang Dai, Harkirat Behl, Jianfeng Wang, Lu Yuan, et al. Generalized decoding for pixel, image, and language. In *CVPR*, 2023. 6

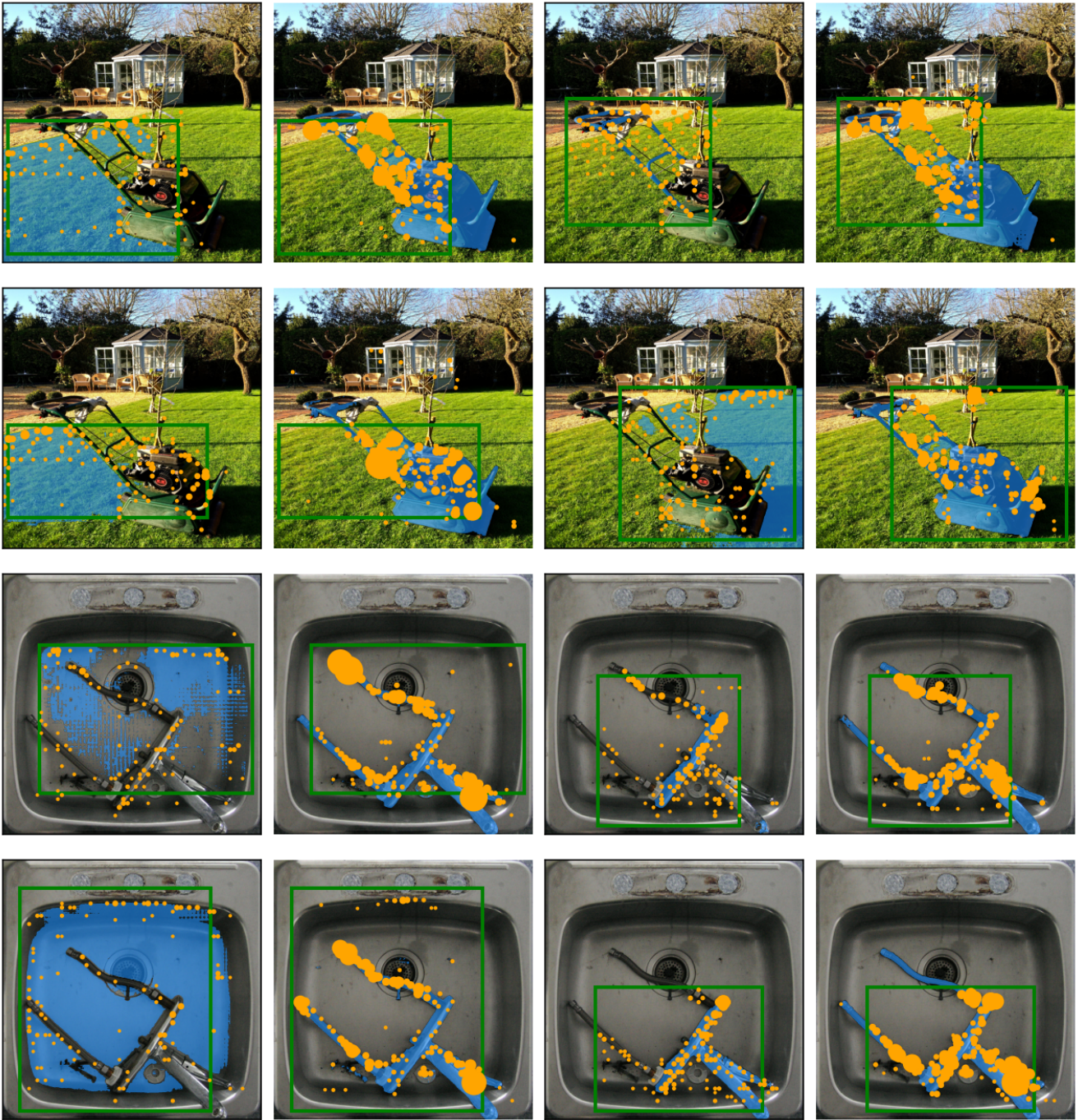


Figure 6. Visual results for box prompts. Within each image pair given the same prompt (green box), the subfigures represent the results of SAM and Stable-SAM, respectively.

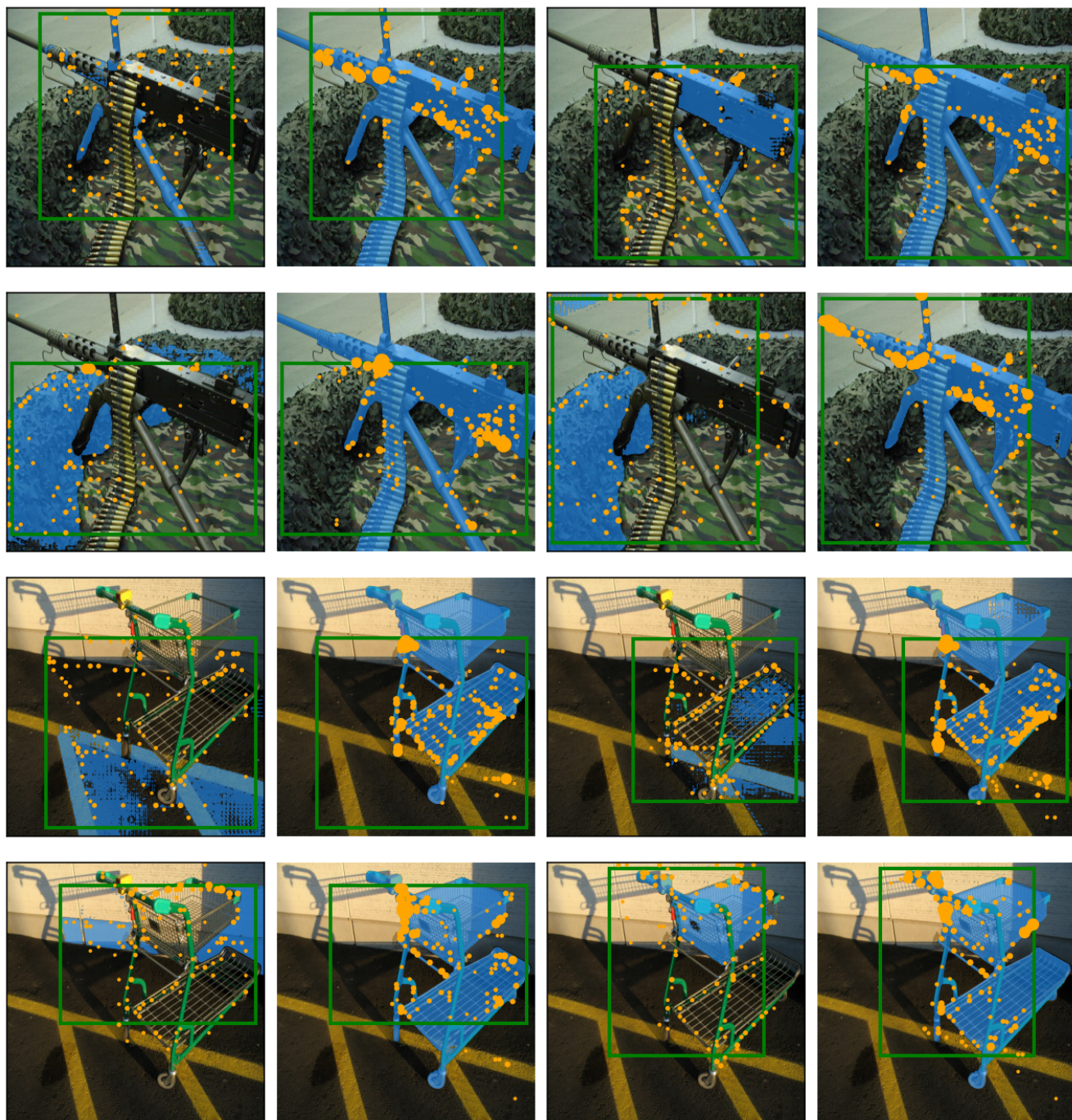


Figure 7. Visual results for box prompts.



Figure 8. Visual results for box prompts.



Figure 9. Visual results for 3-points prompt.

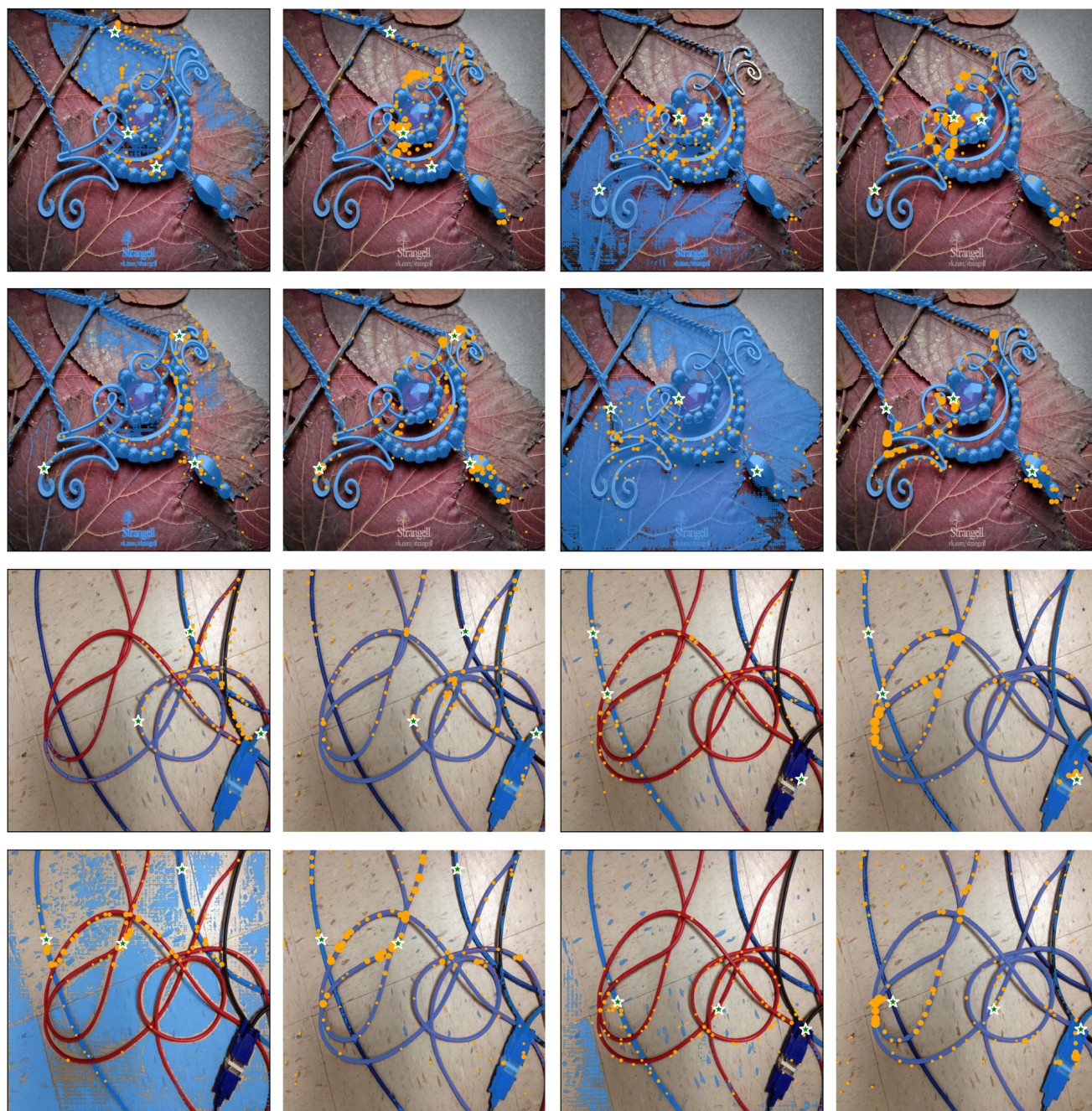


Figure 10. Visual results for 3-points prompt.

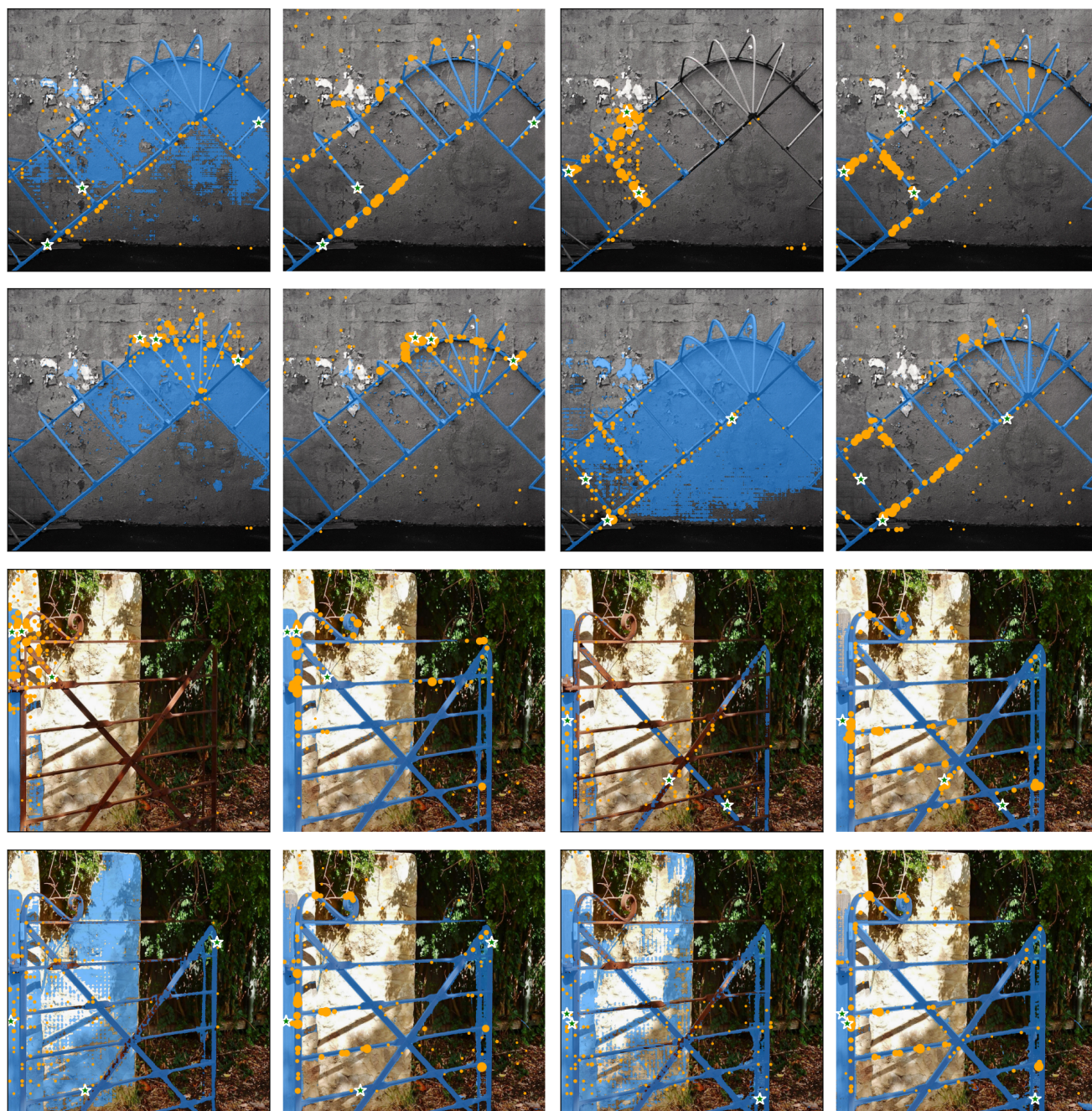


Figure 11. Visual results for 3-points prompt.



Figure 12. Visual results for 1-point prompt.

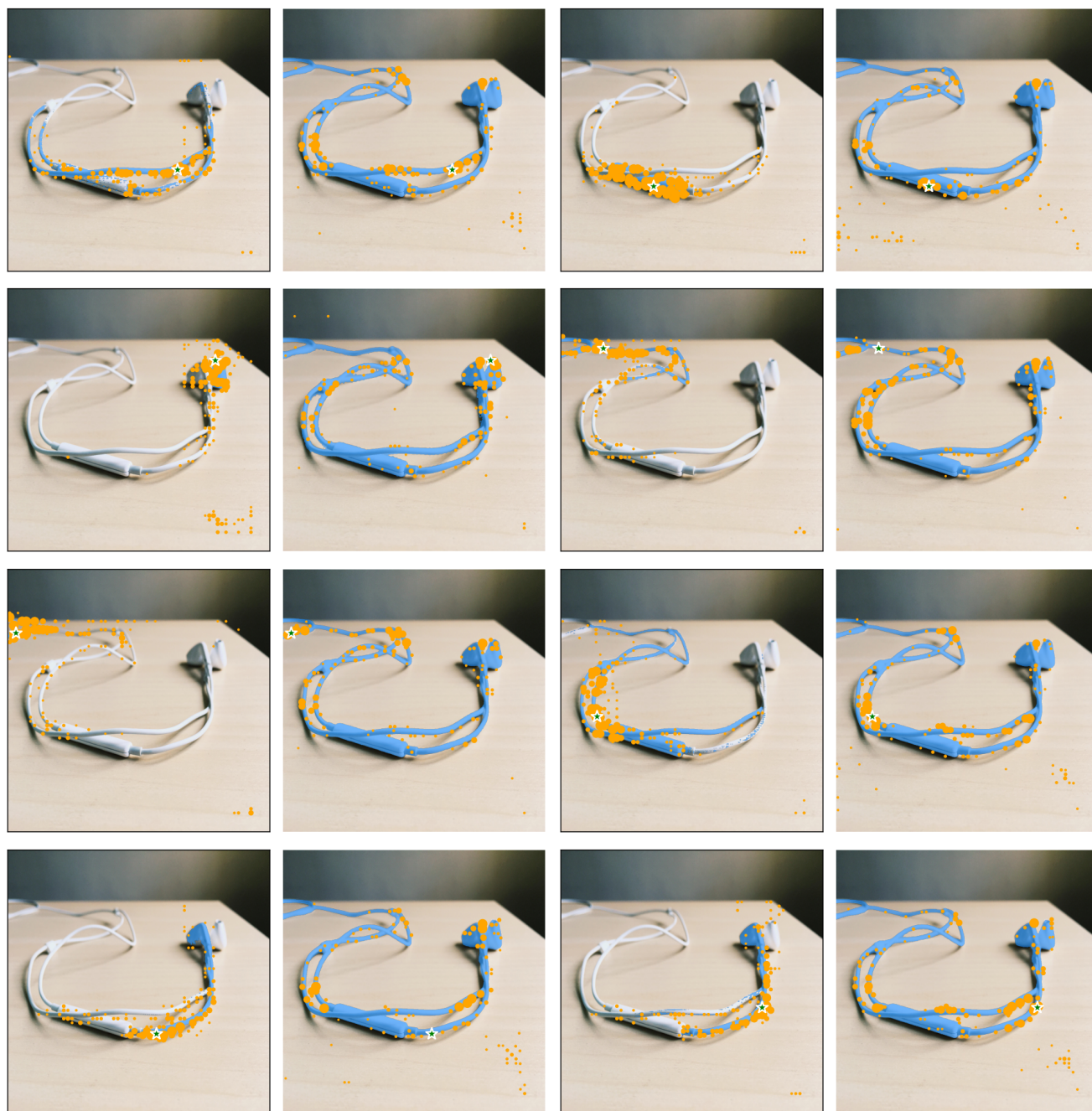


Figure 13. Visual results for 1-point prompt.

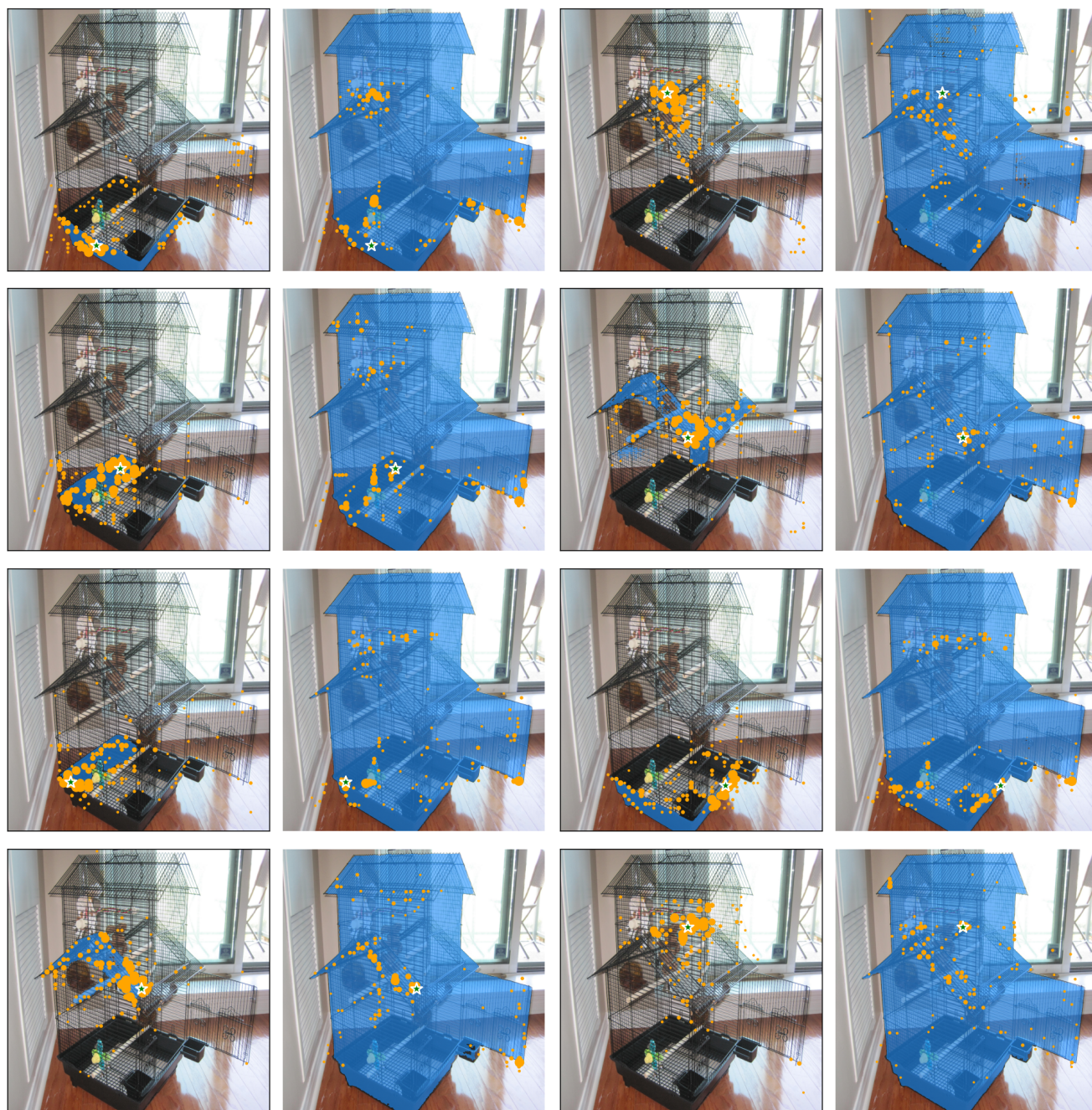


Figure 14. Visual results for 1-point prompt.

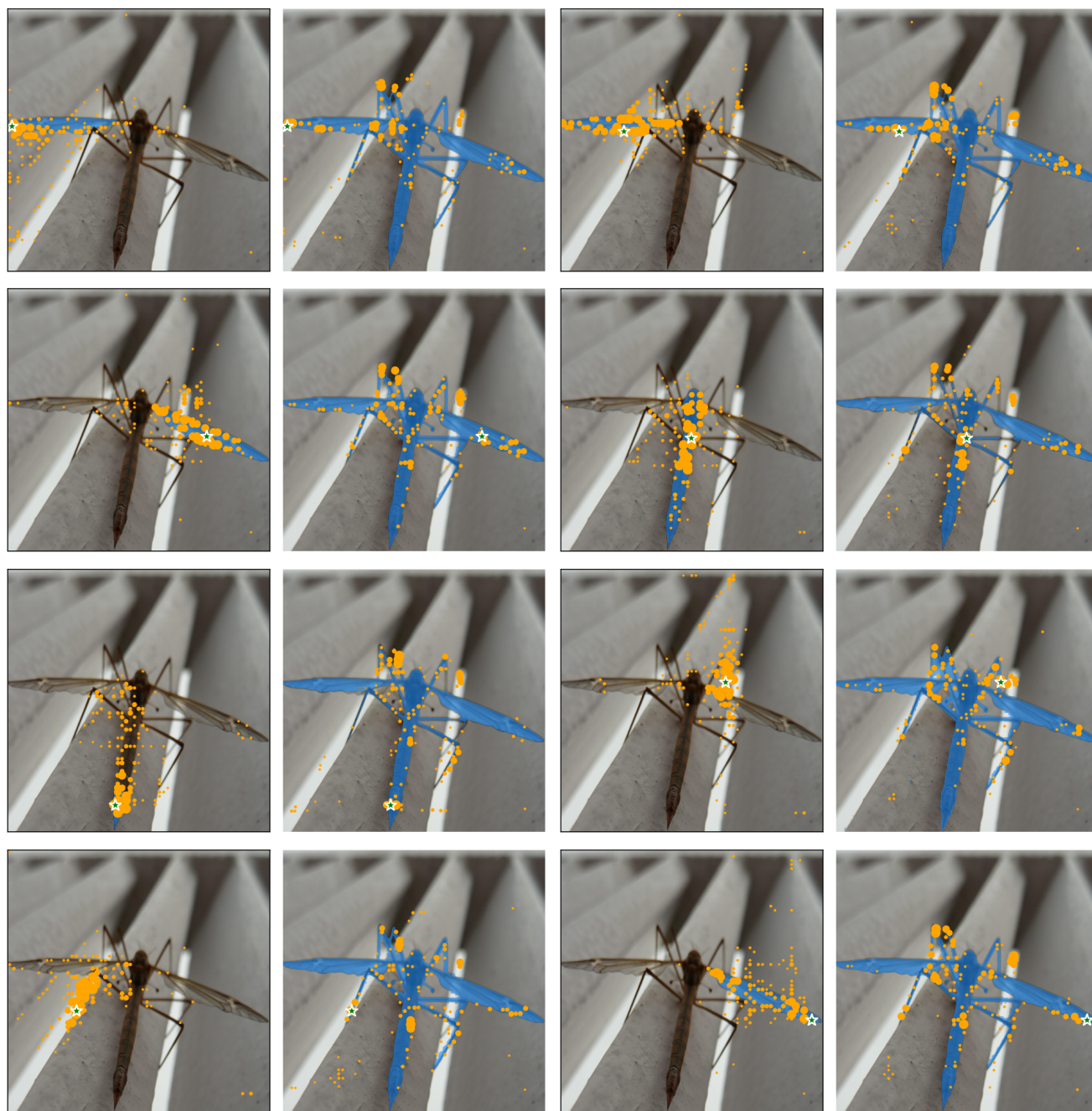


Figure 15. Visual results for 1-point prompt.

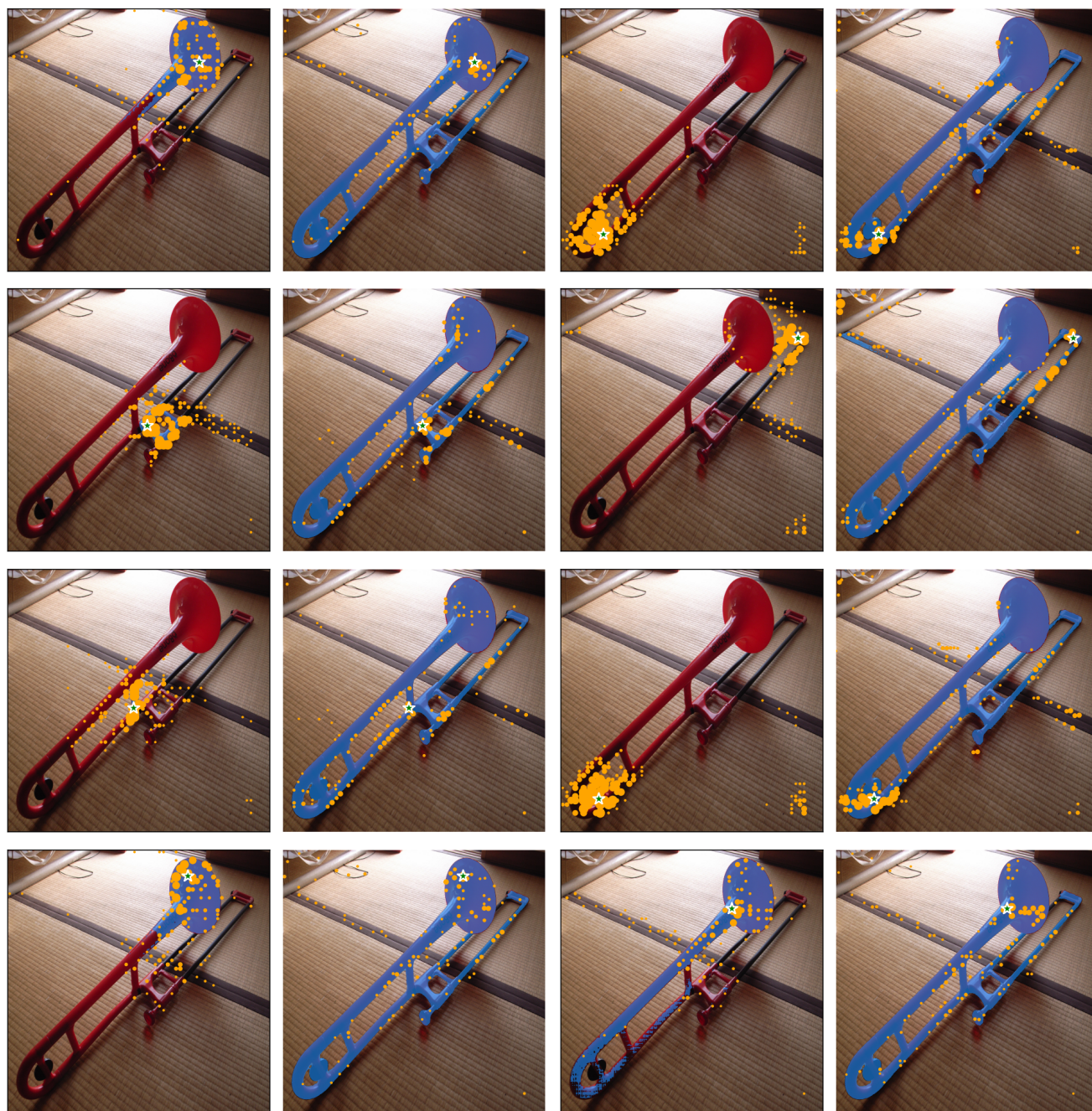


Figure 16. Visual results for 1-point prompt.